BIOCHEMISTRY
including biophysical chemistry & molecular biology

Article

pubs.acs.org/biochemistry

Antigen−Antibody Interactions and Structural Flexibility of a Femtomolar-Affinity Antibody

Hiroaki Fukunishi,*[,†,‡] Jiro Shimada,[†] and Kenji Shiraishi[‡]

[†]Green Innovation Research Laboratories, NEC Corporation, 34, Miyukigaoka, Tsukuba, Ibaraki 305-8501, Japan

[‡]Graduate School of Pure and Applied Sciences, University of Tsukuba, Tennoudai 1-1-1, Tsukuba 305-8571, Japan

Supporting Information

ABSTRACT: The femtomolar-affinity mutant antibody (4M5.3) generated by directed evolution is interesting because of the potential of antibody engineering. In this study, the mutant and its wild type (4-4-20) were compared in terms of antigen−antibody interactions and structural flexibility to elucidate the effects of directed evolution. For this purpose, multiple steered molecular dynamics (SMD) simulations were performed. The pulling forces of SMD simulations elucidated the regions that form strong attractive interactions in the binding pocket. Structural analysis in these regions showed two important mutations for improving attractive interactions. First, mutation of Tyr102(H) to Ser (sequence numbering of Protein Data Bank entry 1FLR) played a role in resolving the steric hindrance on the pathway of the antigen in the binding pocket. Second, mutation of Asp31(H) to His played a role in resolving electrostatic repulsion. Potentials of mean force (PMFs) of both the wild type and the mutant showed landscapes that do not include obvious intermediate states and go directly to the bound state. These landscapes were regarded as funnel-like binding free energy landscapes. Furthermore, the structural flexibility based on the fluctuations of the positions of atoms was analyzed. It was shown that the fluctuations in the positions of the antigen and residues in contact with antigen tend to be smaller in the mutant than in the wild type. This result suggested that structural flexibility decreases as affinity is improved by directed evolution. This suggestion is similar to the relationship between affinity and flexibility for in vivo affinity maturation, which was suggested by Romesberg and co-workers [Jimenez, R., et al. (2003) *Proc. Natl. Acad. Sci. U.S.A. 100*, 92−97]. Consequently, the relationship was found to be applicable up to femotomolar affinity levels.

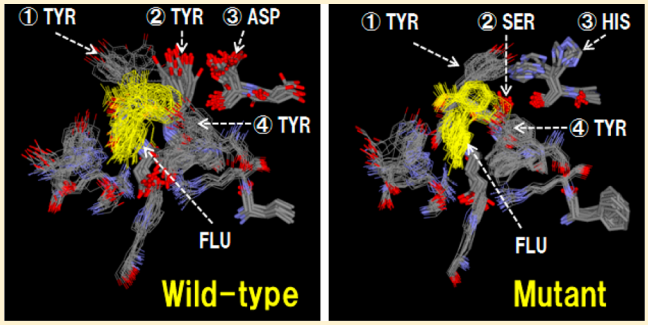

The antibody−antigen reaction is one of the most important molecular recognitions because antibodies play a central role in the immune response.[1−3] Antibodies bind to their antigens with both high affinity and specificity and, thus, serve as excellent targets for investigating molecular recognition. In particular, the anti-fluorescein antibody (4-4-20), which binds to the chromophore fluorescein (FLU) with high affinity, has been widely investigated as a model antibody in terms of its biophysical properties through structural, thermodynamic, kinetic, computational, and mutational analyses.[4−10] The binding affinity (K_d) of the 4-4-20 antibody against the hapten fluorescein−biotin system is 700 pM.[11,12] Romesberg et al. used the 4-4-20 antibody as a model molecule to investigate the mechanism of in vivo antibody evolution from the germ line to the mature antibody (generally termed affinity maturation) using a spectroscopic approach.[13−17] Their results demonstrated that the structural flexibility of a binding site decreases as the affinity is enhanced during affinity maturation and, furthermore, suggested that affinity maturation transforms molecular recognition from an induced-fit model for the germ line into a lock-and-key model for the mature antibody. The induced-fit model indicates that the shape of the antibody is altered in the antigen binding process and polyspecific binding is allowed. On the other hand, the lock-and-key model indicates that the antigen must perfectly fit the antibody; i.e., the binding site is specifically shaped like a lock that fits only a specific keylike antigen. Thorpe and Brooks investigated thermodynamic quantities for the germ line, two intermediates during affinity maturation and a mature antibody (4-4-20), using molecular dynamics (MD) simulations and demonstrated that the binding entropy decreases during affinity maturation.[18] Their results confirmed the relationship between the enhancement of affinity and the decrease in structural flexibility during affinity maturation, as experimentally shown by Romesberg et al. They also discussed the free energy landscape of antibody−antigen binding by expanding the description of a funnel-like energy landscape that is commonly accepted in protein folding.[19−21]

Antibodies play an important role in pharmaceutical and biotechnological industrial applications, such as diagnostics, biosensors, and antibody drugs. Although wild-type antibodies identified by in vivo affinity maturation generally bind with a

Received: June 24, 2011
Revised: March 2, 2012
Published: March 5, 2012

   dx.doi.org/10.1021/bi3000319 | *Biochemistry* 2012, 51, 2597−2605

dissociation constant ranging from 10^{-6} to 10^{-10} M,[22] further improvement in affinity is required for various applications. An anti-fluorescein mutant antibody (4M5.3) was generated by directed evolution, which is a method used in protein engineering, using yeast surface display.[11] The binding affinity was improved 1800-fold relative to that of the wild type (4-4-20), and a K_d of 270 fM was achieved. This binding affinity is the highest in those of antibodies published to date. The mutant contains 14 mutations. Interestingly, this success indicated the potential of antibody engineering in terms of the upper limit for affinity enhancement. Midelfort et al. compared the mutant (4M5.3) with the wild type (4-4-20) by kinetic, thermodynamic, structural, and computational analyses.[12] In comparisons between the crystal structures of the wild type and the mutant, little difference could be observed. The kinetic analyses by stopped-flow techniques showed that the binding kinetics of the mutant and wild type are expressed by single rate constants, so no evidence of the existence of induced fit was provided for either of them. Thermodynamic data and electrostatic energy calculations based on the Poisson−Boltzmann equation furthermore suggested that a large binding free energy change was achieved by the sum of many small structural changes caused by specific mutations that improve electrostatic interactions.

In this study, the femtomolar-affinity mutant antibody (4M5.3) and its wild type (4-4-20) were compared in terms of antigen−antibody interactions and structural flexibility to elucidate the effects of the directed evolution. For this purpose, multiple steered molecular dynamics (SMD) simulations were performed. SMD simulation mimics experimental measurements of pulling a ligand by atomic force microscopy (AFM) but takes place on a different time scale and is quite effective in the investigation of energetic and structural changes between the bound and dissociated states. In the case of nonequilibrium processes such as SMD simulations, Jarzynski equality[23,24] allows us to calculate the binding free energy [termed the potential of mean force (PMF)]. Many researchers have also reported that SMD simulations identified the dynamic processes of protein−ligand binding and unbinding.[25−35] We were especially interested in the relationship between affinity improvement and structural flexibility in directed evolution and, furthermore, the molecular recognition model for the femtomolar-affinity antibody mutant, i.e., induced-fit, lock-and-key, or otherwise. As mentioned above, Romesberg et al.[13−17] and Thorpe and Brooks[18] demonstrated that structural flexibility decreases as affinity is enhanced during in vivo affinity maturation and suggested that molecular recognition is transformed from an induced-fit model into a lock-and-key model. We finally discussed a comparison between in vivo affinity maturation and directed evolution in protein engineering.

METHODS

Structure Preparation. From the Protein Data Bank (PDB), X-ray crystal structures of wild-type 4-4-20 Fab at 1.85 Å resolution (PDB entry 1FLR)[8] and femtomolar-affinity mutant antibody 5M4.3 scFv at 1.50 Å resolution (PDB entry 1X9Q)[12] were taken. The mutant contains 14 mutations relative to the wild type. To properly investigate only the contribution of mutations, equivalent regions were prepared in each crystal structure as follows. After sequences of 1FLR and 1X9Q had been aligned, scFv regions were extracted: residues 1−112 in the light chain and 1−177 in the heavy chain for 1FLR and residues 15−124 and 152−268 for 1X9Q (see Figure S-1 of the Supporting Information). The Cα-rmsd (root-mean-square deviation of Cα atoms) between these regions is 0.8 Å, so the main chains of these regions almost correspond. Missing residues 77 and 78 in 1FLR and 125 and 126 in 1X9Q compensated for each other's structures after these structures were superposed by an rmsd fit of the main chain. Each structure contained an antibody of 219 residues with two disulfide bonds in the heavy and light chains, the antigen of the fluorescein dianion (FLU), and six bound waters in the binding pocket.

To prepare molecular systems for simulation, we added 7994 water molecules (TIP3P) for the wild type and 7994 water molecules and one counterion (Cl^-) for the mutant in cubic simulation boxes automatically by the tleap module in Amber version 9.0. Standard protonation states, including neutral His, were assigned for all residues in all proteins automatically by the tleap module. The force fields of parm99[36] and gaff[37] were assigned for the antibody and for the antigen, respectively. Each system for the wild type and the mutant was minimized for 500 steepest descent steps and 500 conjugate gradient steps. After the minimizations, the systems were heated from 0 to 300 K for 10 ps, during which movements of heavy atoms of the antibody and antigen were restrained with a force constant of 2.0 kcal mol^{-1} $Å^{-2}$. Subsequently, the systems were equilibrated under a constant pressure (*NPT*) for 100 ps, during which all movement of atoms was allowed. In this way, initial structures for simulations were prepared.

Steered Molecular Dynamics (SMD) Simulation. SMD simulation was applied to pull an antigen out of a binding site. This situation mimics experimental measurements of pulling a ligand by atomic force microscopy (AFM). Many researchers also have reported that SMD simulations identified the dynamic processes of protein−ligand binding and unbinding.[25−35] Multiple SMD simulations were performed using Amber version 9. These simulations were performed under the *NVT* condition (300 K), which is controlled by Langevin dynamics with a 1 ps^{-1} collision frequency. SHAKE (rigid bonds)[38] was used on all hydrogen-containing bonds. The particle mesh Ewald (PME) method[39,40] with an 8.0 Å cutoff was used for calculating electrostatic interactions. In addition to general conditions for the MD simulation, conditions for pulling FLU were specified for the SMD simulation. First, a reaction coordinate was specified as the distance between the Cα atom in Val [Val38(H) in PDB entry 1FLR for the wild type or Val188 in PDB entry 1X9Q for the mutant] and the C10 atom in FLU (see Figure 1). The reaction coordinate is termed Val(CA)−FLU(C10). In each SMD simulation, FLU was pulled from 17 to 30 Å on the reaction coordinate. The position at 17 Å indicates a stable distance in the FLU-bound state during 10 ns MD simulations for both the wild type and the mutant (see Figure S-2 of the Supporting Information). The averages were 17.36 Å for the wild type and 17.43 Å for the mutant, and the standard deviations were 0.38 Å for the wild type and 0.37 Å for the mutant. On the other hand, the position at 30 Å indicates a distance completely pulled out of the binding site.

Pulling an antigen corresponds to moving the following guiding potential h:

$$h(\mathbf{r}; \lambda) = \frac{k}{2}[\xi(\mathbf{r}) - \lambda]^2 \quad (1)$$

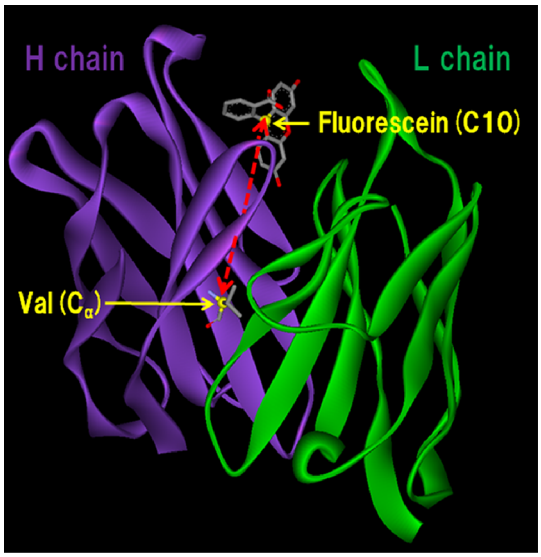

Figure 1. Reaction coordinates for steered MD simulation. The Val(CA)−FLU(C10) coordinate is the distance between the Cα atom of Val in the anti-fluorescein antibody and the C10 atom of fluorescein (FLU). Shown is the crystal structure of the anti-fluorescein mutant antibody (PDB entry 1X9Q), in which Val is residue 188. Purple and green solid ribbons represent heavy and light chains, respectively. The reaction coordinate is represented by a dashed double-headed arrow. During each SMD simulation, FLU moved from 17 Å (bound state) to 30 Å (dissociated state) on the reaction coordinate.

where k, $\mathbf{r}$, and $\xi(\mathbf{r})$ are the spring constant, the three-dimensional coordinate, and the position on the reaction coordinate, respectively. An external parameter λ is changed on the reaction coordinate by a constant velocity v ($\lambda_t = \lambda_0 + vt$, where t is time). Note that $\xi(\mathbf{r})$ is constrained near λ by potential h. In this study, the constant pulling velocity was set to 10 Å/ns. The pulling velocity is an important parameter for SMD simulations because higher pulling velocities may lead to significant nonequilibrium effects, which may introduce obvious errors.[41] Several publications have reported the use of pulling velocities in the range of 10−100 Å/ns.[27,29−35,42,43] Therefore, using a value of 10 Å/ns is reasonable. A large spring constant (k = 20000 kcal mol^{-1} Å^{-2}) was used for stiff-spring approximation,[42] which is described in the next section. Under these conditions, a total of 20 SMD simulations were performed from various initial structures at 17 Å on the Val(CA)−FLU(C10) coordinate for the wild type and the mutant, respectively. Initial structures were generated in 3 ns MD simulations where the Val(CA)−FLU(C10) distance was restrained around 17 Å. Structures were stored every 1 ps, and then 20 initial structures were randomly selected.

Construction of PMF Based on the Jarzynski Equality. The free energy change along a reaction coordinate is termed the potential of mean force (PMF). Generally, the PMF is expressed as a function of coordinate ξ':

$$F(\xi') = -k_B T \ln \int d\mathbf{r}\, d\mathbf{p}\, \delta[\xi(\mathbf{r}) - \xi'] \exp[-\beta H(\mathbf{r}, \mathbf{p})] \tag{2}$$

where ξ and H represent a position on the reaction coordinate and a Hamiltonian of the molecular system, respectively. On the other hand, the PMF based on SMD simulation is expressed by the Hamiltonian of the original system and the guiding potential as a function of external parameter λ correlated to ξ':

$$\begin{aligned}\Phi(\lambda) &= -k_B T \ln \int d\mathbf{r}\, d\mathbf{p} \int d\xi'\, \delta[\xi(\mathbf{r}) - \xi'] \\ &\quad \exp\left\{-\beta H(\mathbf{r}, \mathbf{p}) - \beta\frac{k}{2}[\xi(\mathbf{r}) - \lambda]^2\right\} \\ &= -k_B T \ln \int d\xi' \exp\left[-\beta F(\xi') - \beta\frac{k}{2}(\xi' - \lambda)^2\right]\end{aligned} \tag{3}$$

Note that ξ' is constrained near λ. When spring constant k is significantly large, ξ' is approximated by $\xi' \approx \lambda$ (stiff-spring approximation).[42] Consequently, $\Phi(\lambda) \approx F(\lambda)$; i.e., the free energy of the original system can be expressed as a function of external parameter λ.

The Jarzynski equality[23,24] allows us to calculate free energy changes under nonequilibrium processes such as SMD simulations:

$$\exp(-\beta\Delta F) = \langle \exp(-\beta W) \rangle \tag{4}$$

where ΔF and W represent the free energy change and the work of external force in SMD simulation, respectively, and $\beta = (k_B T)^{-1}$, where k_B and T are the Boltzmann constant and temperature, respectively. The term in broken brackets on the right-hand side is the exponential average, and it is highly possible that insufficient sample data cause large statistical errors. To prevent this problem, the Jarzynski equality is expanded by cumulant expansion as follows:

$$\begin{aligned}\Delta F = \langle W \rangle &- \frac{\beta}{2}(\langle W^2 \rangle - \langle W \rangle^2) \\ &+ \frac{\beta^2}{6}(\langle W^3 \rangle - 3\langle W^2 \rangle \langle W \rangle + 2\langle W \rangle^3) \ldots\end{aligned} \tag{5}$$

and the second-order cumulant is used to suppress statistical error.[42] If the distribution of work W is Gaussian, the third- and higher-order cumulants are identically zero and the second-order cumulant is definitely applicable.[42,44] When the second-order cumulant is used, the free energy change is represented as follows:

$$F(\lambda_t) - F(\lambda_0) = \langle W_{0\to t} \rangle - \frac{\beta}{2}(\langle {W_{0\to t}}^2 \rangle - \langle W_{0\to t} \rangle^2) \tag{6}$$

where λ_t and λ_0 represent positions on the reaction coordinate at time t and time zero, respectively. $W_{0\to t}$ represents the work done from time zero to time t.

The statistical reliability was estimated by the standard deviation obtained by using the bootstrap method.[45] The bootstrap method is generally used for estimating population properties by measuring the empirical distribution of the observed data. The empirical distribution is measured from a number of data sets resampled by random sampling with replacements from the original observed data set. Here, a set of works obtained from N SMD simulations are represented as follows:

$$W_{\text{set}} = \{W^1_{0\to t}, W^2_{0\to t}, W^3_{0\to t}, \ldots, W^N_{0\to t}\} \tag{7}$$

As shown in the textbook about the bootstrap method,[45] the N of 20 used in this study is a workable number. The following

dx.doi.org/10.1021/bi3000319 | Biochemistry 2012, 51, 2597−2605

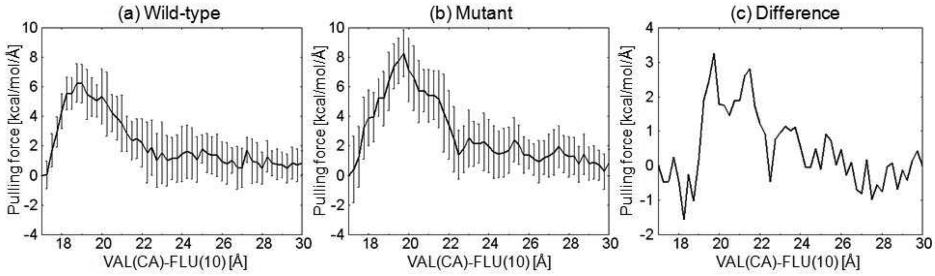

Figure 2. Averages of pulling forces of 20 SMD simulations in the range of 17−30 Å on the Val(CA)−FLU(C10) reaction coordinate for (a) the wild type (4-4-20) and (b) the mutant (4M5.3). Error bars represent standard deviations. Panel c shows the difference between the mutant and the wild type.

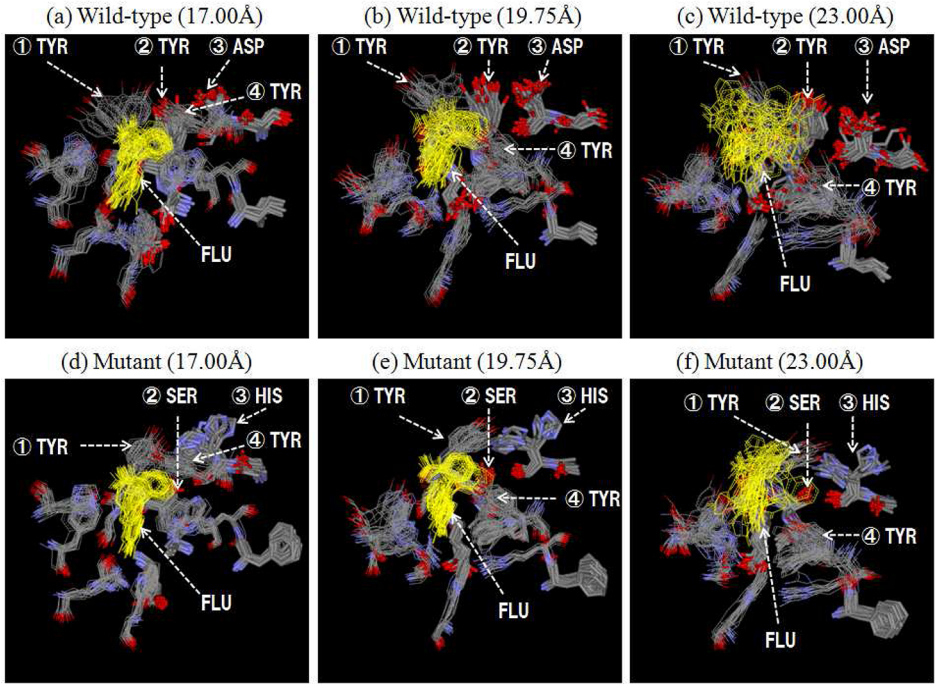

Figure 3. Antibody−antigen interactions for anti-fluorescein antibodies at 17.00, 19.75, and 23.00 Å on the Val(CA)−FLU(C10) reaction coordinate. In each panel, 20 structures obtained by SMD simulations were superposed on the crystal structure by an rms fit of Cα atoms. FLUs are represented by green lines. Residues, in which mutated sites are represented by sticks and otherwise by lines, are colored by atom. Sites 1−4, which are assigned in front of the residue name, correspond to Tyr103(H), Tyr102(H), Asp31(H), and Tyr56(H) in PDB entry 1FLR (wild type) and Tyr254, Ser253, His182, and Tyr207 in PDB entry 1X9Q (mutant), respectively.

set A is generated by random sampling with replacement from W_{set}:

$$A = \{W_{0\to t}^{(1)}, W_{0\to t}^{(2)}, W_{0\to t}^{(3)}, ..., W_{0\to t}^{(N)}\} \quad (8)$$

where $W^{(i)} = W^{(j)}$ $(i \neq j)$ is allowed. Repeating the operation M times generates the following sets (M = 500 in this study):

$$B = \{A^{(1)}, A^{(2)}, A^{(3)}, ..., A^{(M)}\} \quad (9)$$

From each data set $A^{(i)}$ in B, the totals of M PMFs are calculated. The average and the standard deviation of their PMFs are regarded as the estimator and the statistical error, respectively.

RESULTS

Antigen−Antibody Interactions. An external pulling force of the SMD simulation can be obtained throughout the reaction coordinate. The pulling force is calculated by the formula $f_{pull} = \Delta W/\Delta r$, where Δr and ΔW represent changes in the distance and work of pulling FLU in SMD simulation, respectively (Δr = 0.25 A in this study). The values of pulling force are useful for roughly estimating the strength of the interaction between the antibody and FLU throughout the reaction coordinate. Figure 2 compares the average of pulling forces of 20 SMD simulations in the range of 17−30 Å on the Val(CA)−FLU(C10) reaction coordinate between the wild type and the mutant. Note that negative and positive signs denote inward and outward forces in the binding pocket, respectively. In panels a and b, the region of 17−23 Å includes the strong forces for both the wild type and the mutant, and this region is found to be important for antigen−antibody interactions of anti-fluorescein antibodies. On the other hand, the region of 23−30 Å includes the week and nearly flat forces for both the wild type and the mutant. The strongest forces of the wild type and mutant are 6.21 kcal mol^{-1} Å^{-1} at 18.75 Å and 8.23 kcal mol^{-1} Å^{-1} at 19.75 Å, respectively; i.e., the strongest force for the mutant is larger than that for the wild type, and the position the strongest force for the wild type is

dx.doi.org/10.1021/bi3000319 | Biochemistry 2012, 51, 2597−2605

deeper than that for the mutant. Panel c shows the difference in the pulling forces between the mutant and the wild type. This result shows the pulling force for the mutant is stronger than that of the wild type throughout the reaction coordinate except for the range of 17−19 Å; i.e., this result suggests that mutations strengthen attractive antibody−antigen interactions in almost any region. The difference is much larger in the range of 19−22 Å; hence, this region is considered to have a particular effect of mutations.

Figure 3 shows interactions between the anti-fluorescein antibody and FLU antigen on the pathways during 20 SMD simulations for the wild type and the mutant. This figure includes three positions at 17.00, 19.75, and 23.00 Å on the Val(CA)−FLU(C10) reaction coordinate. These three highlighted positions correspond to the initial position in the SMD simulations, the region near the strongest pulling force, and the region changing into a weak and nearly flat force in Figure 2, respectively. In each panel, 20 structures obtained by 20 SMD simulations are superposed on the crystal structure by an rmsd fit between Cα atoms. First, let us look at panels b and e of Figure 3 to confirm antibody−antigen interactions. Note that residue sites 1 and 2, which are assigned in front of the residue name, i.e., Ser253 and Tyr254 in the mutant and Tyr102(H) and Tyr103(H) in the wild type. In the wild type, the two contiguous Tyr residues seem to be quite sterically crowded, especially the side chain of Tyr103(H) that fluctuates significantly. Consequently, their Tyr residues strongly affect the location of FLU by steric hindrance, and FLU also fluctuates significantly. On the other hand, in the mutant, the tightness is relieved because of the substitution with a smaller side chain from Tyr to Ser, and furthermore, the side chain of Tyr successfully fits into the space generated by the substitution. As a result, this mutation plays an important role in resolving steric hindrance on the pathway of FLU. Next, let us look at panels c and f of Figure 3 and confirm antibody−antigen interactions. Note residue site 3, i.e., Asp31(H) in the wild type and His182 in the mutant. This mutation is accompanied by a change in the ionized state. Naturally, Asp with a negative charge in the wild type and dianion FLU repel each other by electrostatic repulsion. On the other hand, His in the mutant plays an important role in resolving the electrostatic repulsion. In Figure 3c, it is seen that the side chain of the His can move readily; i.e., His does not strongly interact with FLU. Next, let us look at panels a and d of Figure 3. Note residue site 4, i.e., Tyr56(H) in the wild type and Tyr207 in the mutant. This site is not a mutation site; however, it is interesting that this Tyr plays a role in capping FLU in the bound state, so the Tyr is considered to significantly affect the binding affinity. As seen in panels b and e of Figure 3 and panels c and f of Figure 3, the Tyr significantly fluctuates except for in the bound state; therefore, the Tyr affects FLU by steric hindrance on the pathway of FLU.

In case of nonequilibrium processes such as SMD simulations, the binding free energy (termed the PMF) can be calculated by the Jarzynski equality. Therefore, we analyzed PMFs of the wild type and the mutant. We first estimated the reliability of PMFs calculated by the second-order cumulant of the Jarzynski equality (see Figure S-3 of the Supporting Information). As a result, we decided that PMFs in the range of 17−30 Å on the Val(CA)−FLU(C10) reaction coordinate are reliable within ±2.5 kcal/mol error bars. Figure 4 compares PMFs between anti-fluorescein wild-type and mutant antibodies. Note that a zero-point origin of PMFs is at 17 Å. The

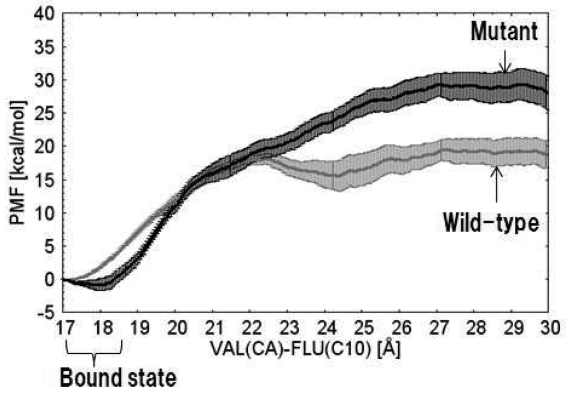

Figure 4. Potentials of mean force (PMF) in the range of 17−30 Å on the Val(CA)−FLU(C10) reaction coordinate. Gray and black lines represent data for the wild type (4-4-20) and mutant (4M5.3), respectively. Error bars correspond to standard deviations obtained from the bootstrap method.

advantage of PMF is that a binding free energy landscape is visualized. First, the smallest values are located at 17.10 Å for the wild type and at 17.90 Å for the mutant; i.e., FLU binds more deeply to the wild type than the mutant. This result is supported by trajectories of the Val(CA)−FLU(C10) distance during 10 ns MD simulations (Figure S-2 of the Supporting Information), in which the Val(CA)−FLU(C10) distance of the wild type tends to be shorter than that of the mutant. The PMF for the mutant goes directly to the bound state from ∼27 Å. On the other hand, the PMF for the wild type is nearly flat between 22 and 30 Å and goes directly to the bound state from ∼22 Å. These results suggest that the mutant starts to stabilize the binding at an earlier stage than the wild type after the two species come close together in a diffusion-controlled process. The landscape that goes directly to the bound state, i.e., does not include intermediate state, has often been described as a funnel-like free energy landscape of protein−ligand interaction.[18,46−48] The kinetic analyses by stopped-flow techniques showed that the binding kinetics of the mutant and wild type are expressed by single rate constants,[12] and this result supports the description of the funnel-like landscape. The funnel-like landscape has been widely accepted for protein folding,[19−21] so it is not difficult to accept for protein−ligand interactions too. Wang et al.[47] theoretically described the funnel-like landscape of a protein−ligand interaction, which was based on protein folding theory.[19] They discussed the idea that forming a funnel-like landscape is related to binding specificity rather than binding affinity, which is derived from just the free energy difference between bound and dissociated states. In accordance with the view of Wang et al., our PMFs support the finding that the wild type and the mutant both have specificity against FLU.

Structural Flexibility. As shown in Figure 3, residues and FLU tended to fluctuate more in the wild type than in the mutant at 19.75 and 23.00 Å on the Val(CA)−FLU(C10) reaction coordinate. Here, it is interesting to quantitatively analyze the change in the fluctuation in position along the reaction coordinate, especially, of mutated sites. The fluctuation in position at each point on the reaction coordinate was calculated from 20 structures obtained by 20 SMD simulations after their structures were superposed on the crystal structure by an rms fit between Cα atoms. Figure 5 compares the magnitudes of fluctuations in the position of the Cα atoms of residues in contact with FLU along the Val(CA)−FLU(C10)

dx.doi.org/10.1021/bi3000319 | *Biochemistry* 2012, 51, 2597−2605

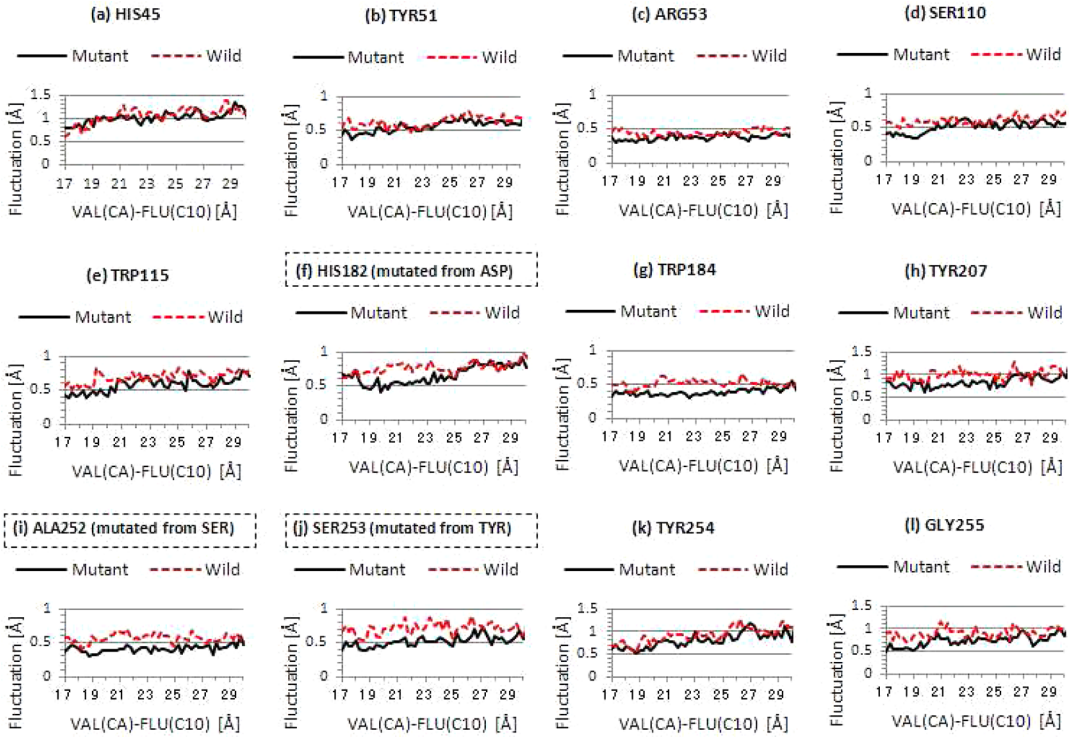

Figure 5. Fluctuations in the positions of Cα atoms in residues contacting FLU along the Val(CA)−FLU(C10) reaction coordinate for anti-fluorescein antibodies. Note that residue numbers in the headings of the panels are those used in PDB entry 1X9Q (mutant). Mutated sites are surrounded by dashed lines. Solid and dashed lines represent data for the mutant (4M5.3) and wild type (4-4-20), respectively. The fluctuation of the position at each point (every 0.25 Å) on the reaction coordinate was calculated from 20 structures obtained by 20 SMD simulations after their structures were superposed on the crystal structure by an rms fit between Cα atoms.

reaction coordinate between the wild type and the mutant. Fluctuations of Cα atoms tend to be smaller in the mutant than in the wild type throughout all residues. As seen in panels f, i, and j of Figure 5, fluctuations of three mutation sites significantly decrease. Interestingly, fluctuations of residues in the heavy chain tend to be larger than those in the light chain. Note that the mutation sites in panels i and j of Figure 5 are in complementarity-determining region CDR-H3. CDR-H3 has various conformations unlike other CDRs[49] and has a crucial role in recognizing the antigen by changing its conformation.[50−52] Our results suggest that mutations for weakening the fluctuation of CDR-H3, i.e., make CDR-H3 more rigid, improve binding affinity. On the other hand, it is also interesting to analyze fluctuations of FLU in the binding pocket. Figure 6 compares the magnitudes of fluctuations in the position of FLU(C10) along the Val(CA)−FLU(C10) reaction coordinate between the wild type and mutant. The fluctuation also tends to be smaller in the mutant than in the wild type throughout the reaction coordinate except for around 27 Å. Here, remember that, in Figure 2, the region of 17−23 Å included the strong pulling forces and was important for antigen−antibody interactions. Combining the results of Figures 2 and 6 shows that FLU always fluctuates less in the mutant than in the wild type in the important region.

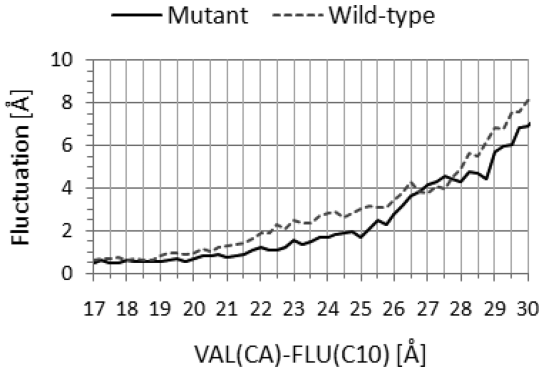

Figure 6. Fluctuations in the position of the C10 atom of fluorosecein (FLU) along the Val(CA)−FLU(C10) reaction coordinate for anti-fluorescein antibodies. Solid and dashed lines represent data for the mutant (4M5.3) and wild type (4-4-20), respectively. The fluctuation in position at each point (every 0.25 Å) on the reaction coordinate was calculated from 20 structures obtained by 20 SMD simulations after their structures were superposed on the crystal structure by an rms fit between Cα atoms.

DISCUSSION

Romesberg et al.[13−17] experimentally and Thorpe and Brooks[18] computationally demonstrated that structural flexibility decreases as binding affinity is enhanced during in vivo affinity maturation and furthermore suggested that molecular recognition is transformed from an induced-fit model for the germ line into a lock-and-key model for the mature antibody. A prototypical induced-fit model provides a flexible antibody that complements the shape of a particular ligand upon binding. The flexibility of the germ line has been related to poly specific binding against various ligands for explaining why the potential number of foreign molecules that can be recognized by the immune system far exceeds the potential number of different antibodies,[15,18] which is limited by available B-cells.[53] On the other hand, the lock-and-key model provides a well-defined

dx.doi.org/10.1021/bi3000319 | Biochemistry 2012, 51, 2597−2605

binding pocket (lock) that is specific for one ligand (key) and prioritizes high affinity over broad specificity.

We also discuss the transformation of the molecular recognition model of affinity improvement from the wild type to the mutant by directed evolution, which is a method used in protein engineering. First, our results demonstrated that fluctuations in positions of residues in contact with FLU tend to be smaller in the mutant than in the wild type; i.e., the antibody seems to behave more as a rigid lock in the mutant than in the wild type. Second, our results demonstrated that the fluctuation in the position of FLU tends to be smaller in the mutant than in the wild type throughout the pathway of FLU in the binding pocket; i.e., the antigen seems to behave more as a rigid key in the mutant than in the wild type. These results suggest that structural flexibility decreases as binding affinity is improved, as well as in vivo affinity maturation, and consequently, this relationship between affinity and flexibility can be applied up to femtomolar affinity levels. Furthermore, these results suggest that the molecular recognition is transformed from a lock-and-key model into a more rigid lock-and-key model by directed evolution. This suggestion is partially supported by results of Midelfort et al., who analyzed the kinetics of binding by stopped-flow techniques.[12] They showed that the binding kinetics of both the mutant and wild type are expressed by single rate constants; i.e., no evidence of the existence of the induced-fit model was provided in either case.

CONCLUSION

We performed multiple SMD simulations for both anti-fluorescein wild-type (4-4-20) and femtomolar-affinity mutant (4M5.3) antibodies and compared the wild type and mutant in terms of antigen−antibody interactions and structural flexibility. The pulling forces of SMD simulations elucidated the regions that engage in strong attractive interactions in the binding pocket. These regions of the wild type and mutant were almost same, but the mutant had mach stronger attractive interactions than the wild type. Therefore, it was found that these regions in particular experience the effect of mutations. Structural analysis in these regions showed two important mutations for improving attractive interactions. First, mutation of Tyr102(H) to Ser (sequence numbering of PDB entry 1FLR) played a role in resolving the steric hindrance on the pathway of the antigen in the binding pocket. Second, it was observed that mutation of Asp31(H) to His plays a role in resolving electrostatic repulsion. To show the electrostatic effect quantitatively, further studies will be required. PMFs were also calculated for estimating the binding free energy change. PMFs of both the wild type and the mutant showed a landscape that does not include obvious intermediate states and goes directly to the bound state. These landscapes were regarded as a funnel-like binding free energy landscape. These PMFs showed that the mutant starts to stabilize the binding at an earlier stage than the wild type after the two species come close together in a diffusion-controlled process.

Next, we analyzed the structural flexibility based on the fluctuations of positions of atoms. It was shown that the fluctuations in the position of the antigen and residues in contact with the antigen tend to be smaller in the mutant than in the wild type. This result suggested that structural flexibility decreases as affinity is improved during directed evolution. This suggestion is similar to the relationship between affinity and flexibility for in vivo affinity maturation, which was suggested by Romesberg et al.[13−17] Consequently, the relationship was found to be applicable up to femtomolar affinity levels. The relationship between affinity and flexibility is expected to be used for development of a high-affinity engineered antibody in pharmaceutical and biotechnological industrial applications such as antibody drugs, biosensors, etc. We consider that estimating the rigid antibody, for example, with a spectroscopic experimental system as conducted by Romesberg et al. may be helpful for efficiently selecting a high-affinity mutant in many candidates.

ASSOCIATED CONTENT

Supporting Information

Aligned sequences of the wild type (PDB entry 1FLR) and the mutant (PDB entry 1X9Q), trajectories of the Val(CA)−FLU(C10) distance during the 10 ns MD simulation, and reliability estimation of PMFs. This material is available free of charge via the Internet at http://pubs.acs.org.

AUTHOR INFORMATION

Corresponding Author

*Phone: +81 29 850 2644. Fax: +81 29 850 6136. E-mail: h-fukunishi@bu.jp.nec.com.

Funding

This work was supported in part by the project on the "Development of Basic Technologies for Advanced Production Methods Using Microorganism Functions" organized by the New Energy and Industrial Technology Development Organization (NEDO).

Notes

The authors declare no competing financial interest.

ACKNOWLEDGMENTS

We thank K. Kamijo (NEC Corp.) for his helpful comments and T. Yagi (NEC Soft, Ltd.) for his helpful advice about Amber.

REFERENCES

(1) Gohlke, H., and Klebe, G. (2002) Approaches to the description and prediction of the binding affinity of small-molecule ligands to macromolecular receptors. *Angew. Chem., Int. Ed. 41*, 2645−2676.

(2) Lazaridis, T. (2002) Binding Affinity and Specificity from Computational Studies. *Curr. Org. Chem. 6*, 1319−1332.

(3) Williams, D. H., Stephens, E., O'Brien, D. P., and Zhou, M. (2004) Understanding noncovalent interactions: Ligand binding energy and catalytic efficiency from ligand-induced reductions in motion within receptors and enzymes. *Angew. Chem., Int. Ed. 43*, 6596−6616.

(4) Herron, J. N., Kranz, D. M., Jameson, D. M., and Voss, E. W. Jr. (1986) Thermodynamic properties of ligand binding by monoclonal anti-fluorescyl antibodies. *Biochemistry 25*, 4602−4609.

(5) Omelyanenko, V. G., Jiskoot, W., and Herron, J. N. (1993) Role of electrostatic interactions in the binding of fluorescein by anti-fluorescein antibody 4-4-20. *Biochemistry 32*, 10423−10429.

(6) Denzin, L. K., Gulliver, G. A., and Voss, E. W. Jr. (1993) Mutational analysis of active site contact residues in anti-fluorescein monoclonal antibody 4-4-20. *Mol. Immunol. 30*, 1331−1345.

(7) Herron, J. N., Terry, A. H., Johnston, S., He, X. M., Guddat, L. W., Voss, E. W. Jr., and Edmundson, A. B. (1994) High resolution structures of the 4-4-20 Fab-fluorescein complex in two solvent systems: Effects of solvent on structure and antigen-binding affinity. *Biophys. J. 67*, 2167−2183.

(8) Whitlow, M., Howard, A. J., Wood, J. F., Voss, E. W. Jr., and Hardman, K. D. (1995) 1.85 Å structure of anti-fluorescein 4-4-20 Fab. *Protein Eng. 8*, 749−761.
(9) Lim, K., and Herron, J. N. (1995) Molecular Dynamics of the Anti-Fluorescein 4-4-20 Antigen-Binding Fragment. 1. Computer Simulations. *Biochemistry 34*, 6962−6974.
(10) Lim, K., Jameson, D. M., Gentry, C. A., and Herron, J. N. (1995) Molecular dynamics of the anti-fluorescein 4-4-20 antigen-binding fragment. 2. Time-resolved fluorescence spectroscopy. *Biochemistry 34*, 6975−6984.
(11) Boder, E. T., Midelfort, K. S., and Wittrup, K. D. (2000) Directed Evolution of Antibody Fragments with Monovalent Femtomolar Antigen-binding Affinity. *Proc. Natl. Acad. Sci. U.S.A. 97*, 10701−10705.
(12) Midelfort, K. S., Hernandez, H. H., Lippow, S. M., Tidor, B., Drennan, C. L., and Wittrup, K. D. (2004) Substantial energetic improvement with minimal structural perturbation in a high affinity mutant antibody. *J. Mol. Biol. 343*, 685−701.
(13) Jimenez, R., Salazar, G., Baldridge, K. K., and Romesberg, F. E. (2003) Flexibility and molecular recognition in the immune system. *Proc. Natl. Acad. Sci. U.S.A. 100*, 92−97.
(14) Jimenez, R., Salazar, G., Yin, J., Joo, T., and Romesberg, F. E. (2004) Protein dynamics and the immunological evolution of molecular recognition. *Proc. Natl. Acad. Sci. U.S.A. 101*, 3803−3808.
(15) Thielges, M. C., Zimmermann, J., Yu, W., Oda, M., and Romesberg, F. E. (2008) Exploring the energy landscape of antibody-antigen complexes: Protein dynamics, flexibility, and molecular recognition. *Biochemistry 47*, 7237−7247.
(16) Zimmermann, J., Oakman, E. L., Thorpe, I. F., Shi, X., Abbyad, P., Brooks, C. L. III, Boxer, S. G., and Romesberg, F. E. (2006) Antibody evolution constrains conformational heterogeneity by tailoring protein dynamics. *Proc. Natl. Acad. Sci. U.S.A. 103*, 13722−13727.
(17) Zimmermann, J., Romesberg, F. E., Brooks, C. L. III, and Thorpe, I. F. (2010) Molecular Description of Flexibility in an Antibody Combining Site. *J. Phys. Chem. B 114*, 7359−7370.
(18) Thorpe, I. F., and Brooks, C. L. III (2007) Molecular evolution of affinity and flexibility in the immune system. *Proc. Natl. Acad. Sci. U.S.A. 104*, 8821−8826.
(19) Bringelson, J. D., and Wolynes, P. G. (1987) Spin glasses and the statistical mechanics of protein folding. *Proc. Natl. Acad. Sci. U.S.A. 84*, 7524−7528.
(20) Onuchic, J. N., Socci, N. D., Luthey-Schulten, Z., and Wolynes, P. G. (1996) Protein folding funnels: The nature of the transition state ensemble. *Folding Des. 1*, 441−450.
(21) Brooks, C. L. III (2002) Protein and peptide folding explored with molecular simulations. *Acc. Chem. Res. 35*, 447−454.
(22) Foote, J., and Eisen, H. N. (1995) Kinetic and affinity limits on antibodies produced during immune responses. *Proc. Natl. Acad. Sci. U.S.A. 92*, 1254−1256.
(23) Jarzynski, C. (1997) Nonequilibrium equality for free energy differences. *Phys. Rev. Lett. 78*, 2690−2693.
(24) Jarzynski, C. (1997) Equilibrium free-energy differences from nonequilibrium measurements: A master-equation approach. *Phys. Rev. E 56*, 5018−5035.
(25) Izrailev, S., Stepaniants, S., Balsera, M., Oono, Y., and Schulten, K. (1997) Molecular dynamics study of unbinding of the avidin-biotin complex. *Biophys. J. 72*, 1568−1581.
(26) Lüdemann, S. K., Lounnas, V., and Wade, R. C. (2000) How do substrates enter and products exit the buried active site of cytochrome P450cam? 2. Steered molecular dynamics and adiabatic mapping of substrate pathways. *J. Mol. Biol. 303*, 813−830.
(27) Xu, Y., Shen, J., Luo, X., Silman, I., Sussmann, J. L., Chen, K., and Jiang, H. (2003) How does Huperzine A enter and leave the binding gorge of acetylcholinesterase? Steered molecular dynamics simulations. *J. Am. Chem. Soc. 125*, 11340−11349.
(28) Gerini, M. F., Roccatano, D., Baciocchi, E., and Nola, A. D. (2003) Molecular dynamics simulations of lignin peroxidase in solution. *Biophys. J. 84*, 3883−3893.
(29) Bayas, M. V., Schulten, K., and Leckband, D. (2003) Forced Detachment of the CD2-CD58 Complex. *Biophys. J. 84*, 2223−2233.
(30) Zhang, D., Gullingsrud, J., and McCammon, J. A. (2006) Potential of mean force for a acetylcholine unbinding from the α7 nicotinic acetylcholine receptor ligand-binding domain. *J. Am. Chem. Soc. 128*, 3019−3026.
(31) Murcia, M., Faraldo-Gomez, J. D., Maxfield, F. R., and Roux, B. (2006) Modeling the structure of the StART domains of MLN64 and StAR proteins in complex with cholesterol. *J. Lipid Res. 47*, 2614−2630.
(32) Xu, Y., Barrantes, F. J., Shen, J., Luo, X., Zhu, W., Chen, K., and Jiang, H. (2006) Blocking of the Nicotinic Acetylcholine Receptor Ion Channel by Chlorpromazine, a Noncompetitive Inhibitor: A Molecular Dynamics Simulation Study. *J. Phys. Chem. B 110*, 20640−20648.
(33) Zou, H., Zheng, M., Luo, X., Zhu, W., Chen, K., Shen, J., and Jiang, H. (2008) Dynamic Mechanism of Fatty Acid Transport across Cellular Membranes through FadL: Molecular Dynamics Simulations. *J. Phys. Chem. B 112*, 13070−13078.
(34) Murcia, M., Jirouskova, M., Li, J., Coller, B. S., and Filizola, M. (2008) Functional and computational studies of the ligand-associated metal binding site of β3 integrins. *Proteins 71*, 1779−1791.
(35) Fukunishi, H., Yagi, H., Kamijo, K., and Shimada, J. (2011) Role of Mutated Residue at the Entrance of the Substrate Access Channel in Cytochrome P450 Engineered for Vitamin D_3 Hydroxylation Activity. *Biochemistry 50*, 8302−8310.
(36) Wang, J. M., Cieplak, P., and Kollman, P. A. (2000) How well does a restrained electrostatic potential (RESP) model perform in calculating conformational energies of organic and biological molecules? *J. Comput. Chem. 21*, 1049−1074.
(37) Wang, J., Wolf, R. M., Caldwell, J. W., Kollamn, P. A., and Case, D. A. (2004) Development and Testing of a General Amber Force Field. *J. Comput. Chem. 25*, 1157−1174.
(38) Ryckaert, J.-P., Ciccotti, G., and Berendsen, H. J. C. (1977) Numerical integration of the Cartesian equations of motion of a system with constraints: Molecular dynamics of n-alkanes. *J. Comput. Phys. 23*, 327−341.
(39) Darden, T., York, D., and Pedersen, L. (1993) Particle Mesh Ewald: An N.Log(N) method for Ewald sums in large systems. *J. Chem. Phys. 98*, 10089−10092.
(40) Essmann, U., Perera, L., Berkowitz, M. L., Darden, T., Lee, H., and Pedersen, L. G. (1995) A smooth particle mesh Ewald potential. *J. Chem. Phys. 103*, 8577−8592.
(41) Isralewitz, B., Gao, M., and Schulten, K. (2001) Steered molecular dynamics and mechanical functions of proteins. *Curr. Opin. Struct. Biol. 11*, 224−230.
(42) Park, S., Khalili-Araghi, F., Tajkhorshid, E., and Schulten, K. (2003) Free energy calculation from nonequilibrium molecular dynamics simulations using Jarzynski's equality. *J. Chem. Phys. 119*, 3559−3566.
(43) Park, S., and Schulten, K. (2004) Calculating potentials of mean force from steered molecular dynamics simulations. *J. Chem. Phys. 120*, 5946−5961.
(44) Hendrix, D. A., and Jarzynski, C. (2001) A "fast growth" method of computing free energy differences. *J. Chem. Phys. 114*, 5974−5981.
(45) Chernick, M. R. (2008) *Bootstrap Methods: A Guide for Practitioners and Researchers*, John Wiley & Sons, New York.
(46) Camacho, C. J., and Vajda, S. (2001) Protein docking along smooth association pathways. *Proc. Natl. Acad. Sci. U.S.A. 98*, 10636−10641.
(47) Wang, J., and Verkhivker, G. M. (2003) Energy Landscape Theory, Funnels, Specificity, and Optimal Criterion of Biomolecular Binding. *Phys. Rev. Lett. 90*, 188101.
(48) Wang, J. (2006) Diffusion and single molecule dynamics on biomolecular interface binding energy landscape. *Chem. Phys. Lett. 418*, 544−548.
(49) Chothia, C., Lesk, A. M., Tramontano, A., Levitt, M., Smith-Gill, S. J., Air, G., Sheriff, S., Padlan, E. A., Davies, D., Tulip, W. R., Colman, P. M., Spinelli, S., Alzari, P. M., and Poljak, R. J. (1989) Conformations of immunoglobulin hypervariable regions. *Nature 342*, 877−883.

(50) Segal, D. M., Padlan, E. A., Cohen, G. H., Rudikoff, S., Potter, M., and Davies, D. R. (1974) The Three-Dimensional Structure of a Phosphorylcholine-Binding Mouse Immunoglobulin Fab and the Nature of the Antigen Binding Sit. *Proc. Natl. Acad. Sci. U.S.A. 71*, 4298−4302.
(51) Sharon, J. (1990) Structural correlates of high antibody affinity: Three engineered amino acid substitutions can increase the affinity of an anti-p-azophenylarsonate antibody 200-fold. *Proc. Natl. Acad. Sci. U.S.A. 87*, 4814−4817.
(52) Wilson, I. A., and Stanfield, R. L. (1994) Antibody-antigen interactions: New structures and new conformational changes. *Curr. Opin. Struct. Biol. 4*, 857−867.
(53) Silverstein, A. M. (2003) Splitting the difference: The germline-somatic mutation debate on generating antibody diversity. *Nat. Immunol. 4*, 829−833.